Available online at www.sciencedirect.com

ScienceDirect

J Materiomics 2 (2016) 316–323

www.ceramsoc.com/en/

www.journals.elsevier.com/journal-of-materiomics/

Enhanced thermoelectric performance of nanostructured CNTs/BiSbTe bulk composite from rapid pressure-quenching induced multi-scale microstructure

Yuewen Zhang, Xiaopeng Jia, Hairui Sun, Bing Sun, Binwu Liu, Haiqiang Liu, Lingjiao Kong, Hongan Ma*

National Key Lab of Superhard Materials, Jilin University, Changchun 130012, China

Received 18 June 2016; revised 26 August 2016; accepted 29 August 2016
Available online 4 September 2016

Abstract

A simple and rapid physical "top-down" pressure-quenching nanostructuring method at high pressure and high temperature (HPHT) was proposed to synthesize *in situ* nanostructured bulk composite material. The multiple and multiscale nanostructures can be spontaneously formed by rapid pressure-quenching from the melt, including the nanocrystals and the lattice disorders. Besides, carbon nanotubes (CNTs) were also dispersed into the material to have more interfaces. The thermal conductivity by the HPHT quenching method is lower than that by other nanostructuring methods, and the minimum value of the material is 0.74 $Wm^{-1}K^{-1}$ at 373 K. The Seebeck coefficient is improved by low energy carrier filtering at grain boundaries and phase interfaces when the electrical conductivity is less deteriorated. The maximum ZT of $Bi_{0.4}Sb_{1.6}Te_3$ bulk material with 0.1 wt.% CNTs is 1.42 at 373 K and 4 GPa. The HPHT quenching method can provide a promising alternative to obtain nanostructured bulk composite materials with the enhanced thermoelectric performance.

Keywords: Thermoelectric; High pressure; Bi_2Te_3; Quenching; Defect; Full-spectrum phonon scattering

1. Introduction

Energy dilemma and environmental concerns accelerate the development and application of thermoelectric (TE) materials [1]. The TE devices exhibit distinct advantages in some applications such as micro-coolers, micro-power generations, and space-crafts. However, the conversion efficiency, i.e., figure of merit ($ZT = S^2\sigma T/\kappa$), is so low that the TE devices are incapable of competing with conventional energy supply in commercial applications. The difficulty in the TE performance enhancement is how to mutually optimize the three parameters (i.e., S, σ and κ) on their interactions and contradictions. Some recent strategies for nanostructuring and band engineering show a potential to achieve the enhanced TE performance by decoupling the interdependence [2,3]. Nanostructuring is regarded as an effective approach to increase the power factor and reduce the lattice thermal conductivity [2,4,5]. In the low-dimensional (i.e., 0 D to 2D) systems, such as nanodots, nanowires and superlattices, the Seebeck coefficient is increased from both the low energy carrier filtering effect and the quantum confinement effect (i.e., high density of electronic states). Meanwhile, the lattice thermal conductivity is reduced by phonon scattering from a high density of interfaces. Venkatasubramanian et al. obtained a high ZT value of 2.4 on Bi_2Te_3/Sb_2Te_3 superlattice device by quantum confinement effect of carrier transport [6]. Harman et al. reported a lattice thermal conductivity of 0.33 W/mK on a cooling device, which was benefited from quantum dot in PbTe/PbSe matrix [7]. In addition, some nanocomposites with nanoparticles [8]

* Corresponding author. Fax: +86 431 85168858.
E-mail address: maha@jlu.edu.cn (H. Ma).
Peer review under responsibility of The Chinese Ceramic Society.

http://dx.doi.org/10.1016/j.jmat.2016.08.002

and nanotubes [9] were also developed to effectively enhance the TE properties and demonstrate some prospects for the practical applications.

Since the validity of nanostructuring is attributed to the reduced grain size and intensive boundary, the problem is how to fabricate the nanostructures. In general, there are two routes, i.e., a) a "bottom-up" approach usually produces nanoparticles by melt spinning, milling or hydrothermal/solvothermal method, which are treated in HP or SPS to obtain bulk materials, and b) a "top-down" approach deconstructs bulk materials into nanoscale. Many chemical top-down routes have been applied to produce nanoporous and ordered arrays, such as thermal decomposition and anisotropic dissolution [10]. Besides, a physical top-down method is also an alternative to achieve nanofabrication. Hot deformation method produces *in situ* nanostructures *via* recrystallization to enhance the TE properties [11]. The physical top-down route is more simple and time-saving without pre- and post-treatment. However, it is less explored so far. High cooling rate can fabricate nanostructured features, such as melt spinning [12]. Moreover, quenching at a high pressure can further intensify the effects of high cooling rate [13,14].

As the dominant TE materials at near room temperature, Bi_2Te_3-based derivatives show a bottleneck of ZT ~1 for decades. The zone melting ingots are restricted to anisotropic properties and weak mechanical strength. Therefore, it is necessary to fabricate Bi_2Te_3-based bulk materials with the enhanced isotropic TE performances for commercial applications. Carbon nanotubes (CNTs) intrinsically exhibit a high carrier mobility and a high electrical conductivity. In addition, the dispersed CNTs in thermoelectric matrix can enhance the phonon scattering at interfaces. Some investigations indicated that the dispersion of CNTs or fullerene could increase the interfaces, refine the microstructure and improve the TE performance [15,16].

In this paper, a simple, rapid and feasible high-pressure and high-temperature (HPHT) method was applied as a "top-down" strategy for the synthesis of BiSbTe composite material [17]. The CNTs-composited polycrystalline BiSbTe nanostructured bulk materials were directly synthesized. Also, the microstructures were generated by the HPHT quenching method at a high cooling rate.

2. Experimental

2.1. Sample synthesis

The samples were synthesized by high pressure and high temperature (HPHT) synthesis and subsequent high pressure sintering (HPS). In the HPHT synthesis, commercial powders of Bi, Sb and Te elements (5 N) and CNTs were used as starting materials. The powdered chemicals with the compositions of CNTs 0.1 wt% and $Bi_{0.4}Sb_{1.6}Te_3$ were cold pressed into cylinders (ø 10.5 × 4 mm) after they were mixed and ground in Ar atmosphere. The cylinders were assembled into chambers for the subsequent HPHT synthesis (2 GPa, 890 K; 3 GPa, 910 K; 4 GPa, 930 K for 25 min) on China-type large volume cubic high-pressure apparatus (CHPA) (SPD-6 × 1200). The sample chamber was heated by a graphite crucible and pressurized by a hydraulic pressed multianvil technique. The temperature was measured by a thermocouple on the sample surface and the pressure was gauged by a calibration curve from resistance change of standard materials. Since the chamber contacts with the water-cooled WC anvils and large volume hydraulic cylinders, the rapid "pressure-quenching" is implemented by cutting heating current immediately. The chamber was decompressed from synthetic pressure to ambient pressure within one minute after quenched to room temperature at a high cooling rate of 400 K/min. The HPHT samples were obtained. In the HPS synthesis, to avoid the TE performance overestimation by anisotropy [18], a batch of HPHT samples were smashed and ground thoroughly into powders, and sintered into a cylinder (ø10.5 × 12 mm) at the corresponding synthetic pressure at 625 K for 5 min. A disk of ø10 × 2 mm and a bar of 2 × 2 × 8 mm were cut along the axial direction of HPS sample for the TE property measurements. Fig. 1 shows the synthesis procedure.

2.2. Characterization

The crystal structure of the samples was determined by X-ray diffraction on a model D/MAX-RA diffractometer (Rigaku Co., Japan). The morphology and microstructure were observed by a model JSM-6700F field emission scanning electron microscope (JEOL Co., Japan) and a model JEM-2200FS high-resolution transmission electron microscope (JEOL Co., Japan). The bar-shaped sample was used for the measurements of the Seebeck coefficient and electrical resistivity simultaneously at 323–523 K by ZEM-3 (Ulvac-Riko Co., Japan). The thermal diffusivity (λ) was determined by a model LFA-427 laser flash instrument (Netzsch Co., Germany). The volume density (d) was measured by the Archimedes method. The heat capacity (C_p) was performed on STA PT-1750 by DSC conversion (Linseis Co., Germany) with a sapphire standard sample for calibration. The total thermal conductivity (κ) was determined *via* the relationship of thermal diffusivity, volume density, and specific heat (i.e., $\kappa = \lambda d C_p$). The error rate of the Seebeck coefficient, electrical resistivity, and thermal conductivity is 3%, 5% and 10%, respectively. The calculated power factor and ZT values have the error rates of 11% and 21% $\left(\text{based on}\left|\frac{\Delta Z}{Z}\right| = 2\left|\frac{\Delta S}{S}\right| + \left|\frac{\Delta\sigma}{\sigma}\right| + \left|\frac{\Delta\lambda}{\lambda}\right| + \left|\frac{\Delta d}{d}\right| + \left|\frac{\Delta C_P}{C_P}\right|\right)$ [19].

3. Results and discussion

3.1. XRD spectra, morphology and microstructure

Fig. 2 shows the XRD spectra of HPS samples. Clearly, all the diffraction spectra can be indexed to the standard pattern of $Bi_{0.4}Sb_{1.6}Te_3$ (JCPDS 72–1836). No detectable diffraction peak of CNTs appears due to the low content. Compared to the

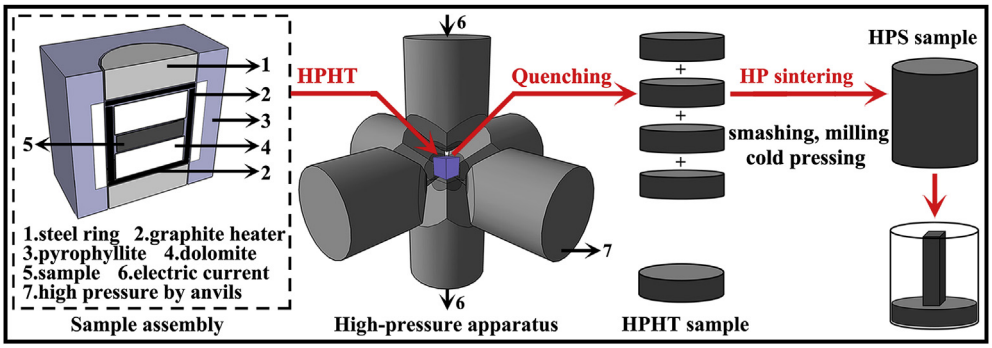

Fig. 1. Procedure of nanostructured bulk materials synthesized by HPHT synthesis (sample assembly, high-pressure apparatus) and high pressure sintering (HPS).

standard pattern, no preferential grain orientation appears from the relative intensities of (00l) planes. Therefore, no grain anisotropy in the sample exists after the HPS process due to smashing and fine milling. The results indicate that polycrystalline nanocomposite $Bi_{0.4}Sb_{1.6}Te_3$ bulk material can be synthesized by the simple and rapid HPHT and HPS method in 30 min.

Fig. 3a and b shows the typical FESEM images of HPHT and HPS samples. The morphology of HPHT bulk shows a typical lamellar structure. There are some aggregates of the well-crystallized grain sheets with the sizes of tens of μm. Also, some coarse grain particles distribute among the sheets (see Fig. 3a). This lamellar morphology is due to the layered crystal structure of Bi_2Te_3 and the two-dimensional nucleation/growth as well as the relative slippage by shearing (see Fig. 3c). The HPHT method can be applied to synthesize the fine-grained bulk materials in just 25 min. However, the presence of large sheets will lead to the anisotropy in the TE performance. It is thus necessary to eliminate the large sheets by smashing and milling. In Fig. 3b, the particle size of HPS sample is distinctly reduced, but the lamellar structure is still retained after the HPS. Based on the XRD results, no grain anisotropy of preferential orientation occurs after the HPS treatment.

Fig. 4 shows the HRTEM images of the multiple microstructures in the samples. Clearly, there are many characteristic nanocrystals with clear lattice planes (see Fig. 4a and b). However, other structures exhibit amorphous with a low crystallinity (marked by A). The average size of nanocrystals at 4 GPa is slightly smaller than that at 2 GPa, leading to the more scattered amorphous microstructures and the more abundant boundaries. Meanwhile, the disorder of lattice orientation is more remarkable at a higher pressure [14]. This morphology should be related to the nucleation/growth rate by quenching at different pressures. A high cooling rate of quenching will increase the nucleation rate and will decrease the critical nucleation radius and the growth rate. Also, a higher pressure can reduce the critical nucleation radius, promote the nucleation and suppress the growth of nuclei due to the restrain of atom movement [13,20]. This implies that the introduction of high pressure intensifies the quenching effect, giving the smaller nanocrystal size and more random aligned nanocrystals [13].

In addition to the nanocrystals, some other microstructures appear (see Fig. 4c–f). The lattice curvatures and dislocations are induced by a high pressure strain. The precipitation, fringes, and stacking faults in the matrix could result from the inhomogeneous chemical compositions by quenching or lattice planes twist/shift at a high pressure. The multiple and multiscale microstructures can produce the perturbations in lattice periodicity, resulting in a full-spectrum phonon scattering to reduce the thermal conductivity.

Fig. 5 shows the dispersion of CNTs in BiSbTe matrix by HPHT. The CNTs have the diameters of approximately 30–50 nm. The dispersed CNTs mainly distribute at the boundaries of grain sheets. The enlarged image distinctly reveals the CNTs attached on the surfaces of grain sheets (see Fig. 5b). The dispersion of CNTs certainly introduces the CNT/matrix phase interfaces to impede the phonon propagation.

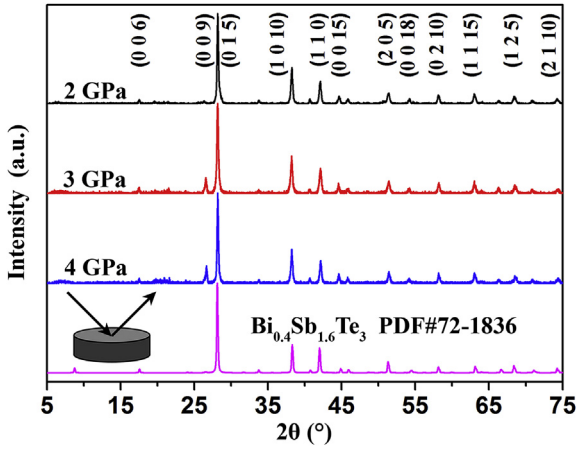

Fig. 2. XRD patterns of HPS samples at different synthetic pressures.

3.2. Thermoelectric properties

Fig. 6 shows the temperature-dependent electrical transport properties of the samples at different pressures. The Seebeck coefficient indicates p-type transport with holes as dominant charge carriers. The positive temperature dependence of electrical resistivity exhibits a degenerated semiconductor behavior. The Seebeck coefficient and electrical resistivity

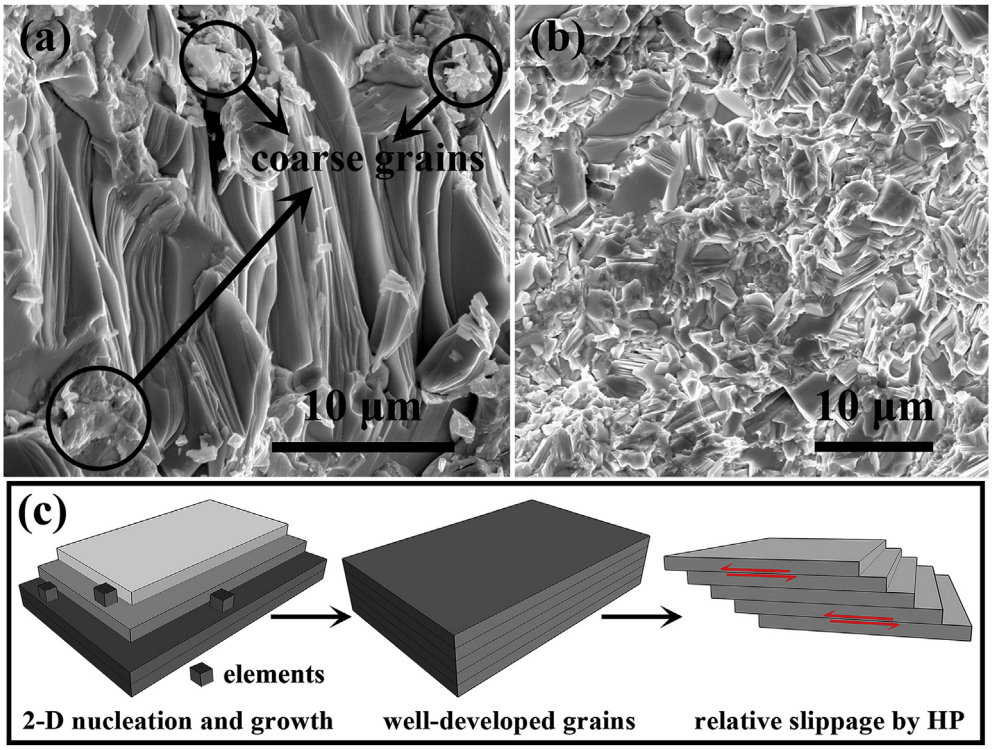

Fig. 3. Typical FESEM images of samples by HPHT method and after high pressure sintering process: (a) HPHT sample, (b) HPS sample, (c) Schematic of two-dimensional nucleation and relative slippage.

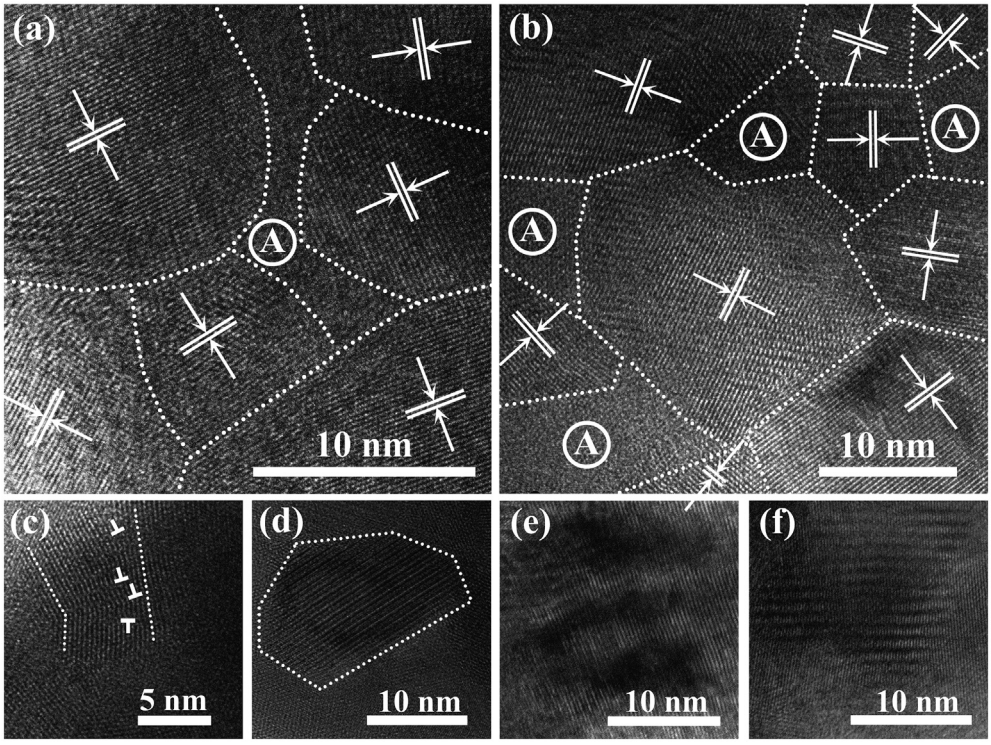

Fig. 4. HRTEM images of multiple microstructures. Nanocrystals and amorphous structures of 2 GPa (a) and 4 GPa (b) (c–f). The microstructures such as dislocations, precipitation, fringes, and stacking faults.

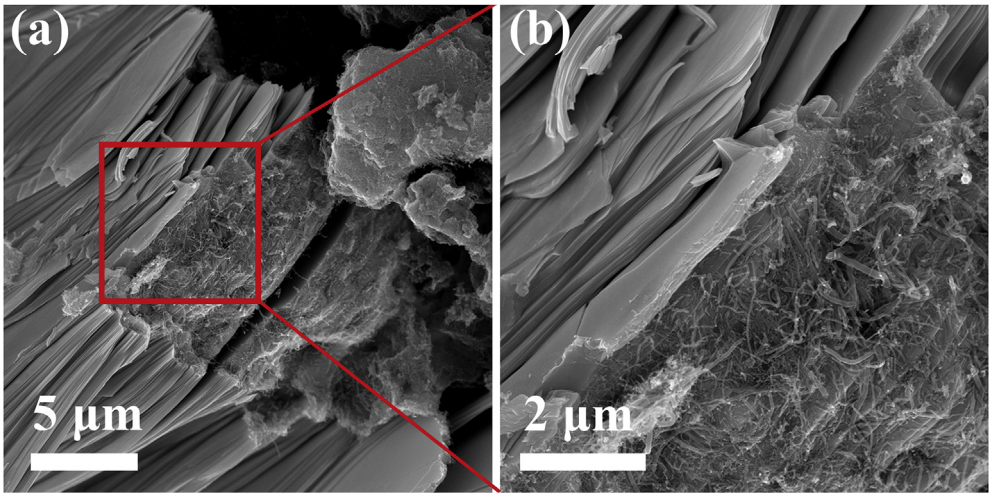

Fig. 5. Dispersion of CNTs in the HPHT sample matrix and the corresponding enlarged image.

both increase with increasing pressure. This reveals that the more abundant microstructures at a higher pressure can decrease the mobility of carriers and increase the scatter factor. The maximum Seebeck coefficient (marked by arrows) shifts to a higher temperature range as pressure decreases. The reason is that a low value of the Seebeck coefficient usually has a relatively high level of carrier concentration, which will suppress the minor carrier excitation due to the bipolar effect. As a result, the peak moves towards a higher temperature range [21,22]. Table 1 shows the details of carrier transport at room temperature to survey the high pressure effect. The carrier concentration and mobility both decrease with increasing synthetic pressure, which are consistent with the variations of the Seebeck coefficient and electrical resistivity. Fig. 6c shows the calculated power factor. The power factor values are distinctly improved by pressure due to the increased Seebeck coefficient. The use of higher pressure is beneficial for the improvement of electrical transport properties. The maximum PF value at 323 K is 31.83 $\times$ 10^{-4} $Wm^{-1}K^{-2}$ for the nanostructured sample at 4 GPa.

Fig. 7 shows the temperature-dependent thermal conductivity and the ZT values at various synthetic pressures. The thermal conductivity decreases from 1.31 and 0.95 to 0.78 $Wm^{-1}K^{-1}$ at 323 K as the synthetic pressure increases

Table 1
Hall coefficient (R_H), carrier concentration (p), carrier mobility (μ) and electrical resistivity (ρ) of samples at different synthetic pressure at 300 K.

Samples	R_H (cm^3C^{-1})	p (10^{19} cm^{-3})	μ ($cm^2V^{-1}S^{-1}$)	ρ (10^{-6} Ω m)
2 GPa	0.14	4.46	349	4.01
3 GPa	0.17	3.68	272	6.25
4 GPa	0.23	2.72	254	9.03

from 2 to 4 GPa. The considerable increase at a high temperature is due to the bipolar effect near the intrinsic excitation region, particularly for the sample at 3 and 4 GPa with a relatively low carrier concentration. The minimum thermal conductivity is 0.74 $Wm^{-1}K^{-1}$ at 373 K for the sample at 4 GPa. The ZT values are obtained to evaluate the overall effects of pressure-quenching. The ZT improvement is achieved by a higher pressure. The sample at 4 GPa exhibits an enhanced ZT value of 1.42 at 373 K. This impressive gain stems from the relatively high Seebeck coefficient and the distinctly reduced thermal conductivity. Table 2 shows some investigations on BiSbTe materials by various nanostructuring methods. Kim et al. developed a liquid-phase-compaction method to form dense dislocation arrays, and obtained a remarkable high ZT value of 1.86 at 320 K for $Bi_{0.5}Sb_{1.5}Te_3$ [23]. Poudel et al. obtained a ZT value of 1.4 at 373 K in

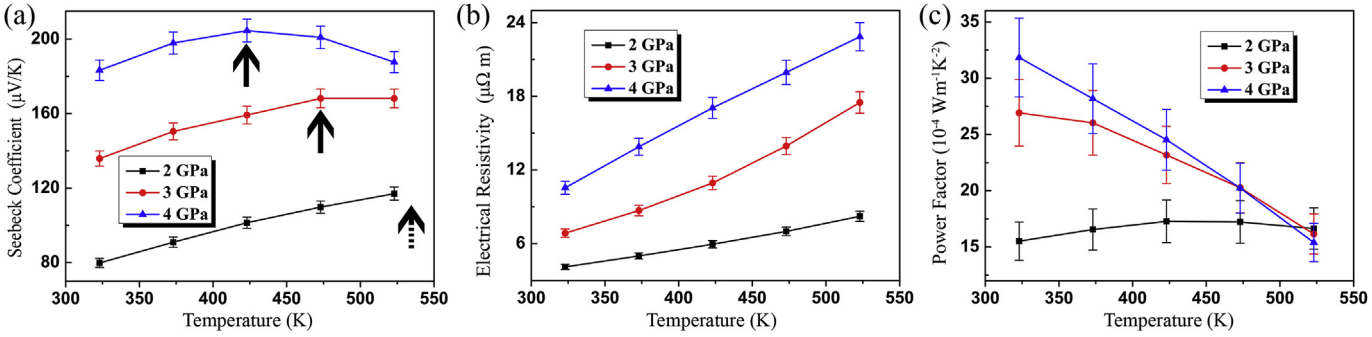

Fig. 6. Temperature dependence of thermoelectric properties of HPS samples (a) the Seebeck coefficient, (b) electrical resistivity, and (c) power factor.

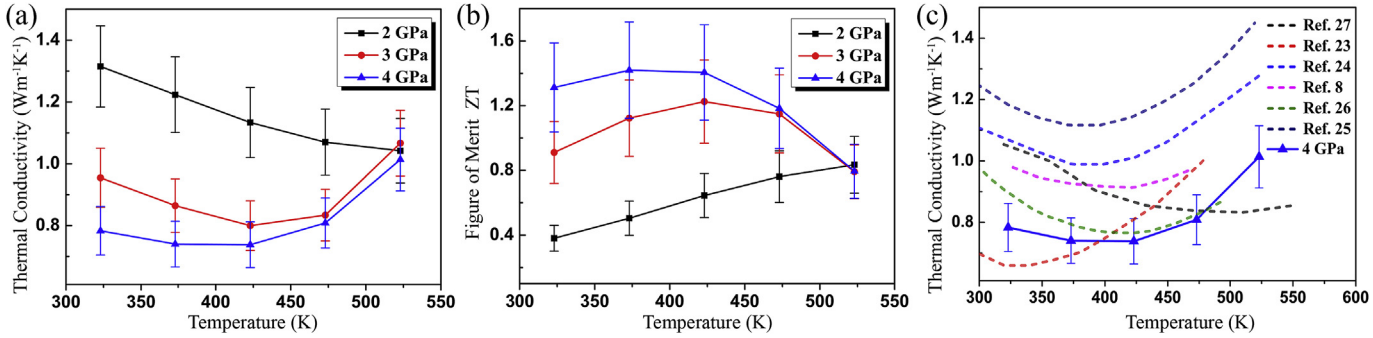

Fig. 7. (a) Thermal conductivities and (b) The ZT values at different temperatures; (c) The temperature-dependent thermal conductivity from nanostructured bulks by various nanostructuring methods.

BiSbTe nanocrystalline bulk by ball-milling and hot pressing from commercial alloy ingot, which resulted from grain boundaries and defects scattering [24]. Similarly, Ma et al. achieved a ZT value of 1.3 at 348–373 K by the same nanostructuring approach with elemental chunks as starting materials [25]. Li et al. reported an improved ZT value of 1.33 at 373 K for $Bi_{0.3}Sb_{1.7}Te_3$ by SiC nanoparticles, which resulted in the reduction of lattice thermal conductivity [8]. $BiSbTe_3$ bulks by Cao et al. *via* a hydrothermal route and a hot pressing had a high ZT value of 1.47 at 443 K [26]. Xie et al. obtained a ZT value of 1.56 at 300 K when they used a melt spinning/spark plasma sintering technique [12]. In a previous work, we obtained a ZT value of 1.3 at 510 K in $Bi_{0.5}Sb_{1.5}Te_3$ bulk through a high-pressure synthesis (at 3.8 GPa) [27]. The enhancement of the ZT value in this work indicates that pressure-quenching could be effective to fabricate the high-performance nanostructured bulk materials.

However, the thermal conductivity by pressure-quenching is slightly lower than that of the nanostructured bulk samples by other nanostructuring methods (see Fig. 7c). The thermal conductivity of CNTs-composited sample is lower than that of no CNTs sample [27]. In general, the lattice thermal conductivity can be qualitatively expressed as: [23,28].

$$\kappa_L = \frac{1}{3} C v l = \frac{1}{3} C v^2 \tau \quad (l = v\tau) \tag{1}$$

where C, v, l and τ are specific heat, speed of sound, phonon mean free path, and phonon relaxation time, respectively. However, it is assumed that all the parameters should have no temperature and frequency dependences. Actually, the heat conduction is carried out by a whole spectrum of phonons at various frequencies (ω). The integral of frequency-dependent κ_L is described as: [23,28].

$$\kappa_L = \frac{1}{3} \int C(\omega) v^2(\omega)\ \tau(\omega)\, d\omega \tag{2}$$

Since specific heat and speed of sound vary slightly for a given material, it is crucial to tailor phonon relaxation time by introducing various phonon scattering mechanisms so as to obtain a low lattice thermal conductivity. However, the lattice thermal conductivity will be near zero if the Wiedemann–-Franz law is used, which is physically impossible. Some investigations also reported that the common Lorentz number could not apply to the situations such as nanostructured bulk material, the resonant level enhancement and high electronic density of states [29,30]. High pressure can generate both distinct band alterations and plenty of micro-/nano-structures, which may result in novel transport behaviors. However, the reason for the abnormal lattice thermal conductivity for HPHT sample is needed to be further clarified.

Fig. 8 shows the schematic diagram of microstructures to elucidate the effect of multiple microstructures on the phonon and carrier transport from hot to cold junction. The microstructures are divided into four scales. **(1) Atomic scale**, including point defects and dislocations. The antisite defects (Bi_{Te} and Sb_{Te}) and Te vacancies (V_{Te}) are also common point defects in Bi_2Te_3–based materials. Besides, there are abundant pressure-induced dislocations. The atomic scale defects mainly scatter high-frequency/short-wavelength phonons as the frequency dependence of relaxation time is $\tau_P^{-1} \sim \omega^4$; **(2) Nanoscale scale**, including nanocrystal, precipitation, fringe, and stacking fault. The microstructures in

Table 2
TE bulks with enhanced performances by different nanostructuring methods.

Sample	Nanostructuring method	ZT_{max}		Reference
$Bi_{0.5}Sb_{1.5}Te_3$	Melt spinning + SPS (liquid-phase-compaction)	1.86	320 K	Ref. [23]
$(Bi, Sb)_2Te_3$	Ball milling (ingot) + hot pressing	1.4	373 K	Ref. [24]
$(Bi, Sb)_2Te_3$	Ball milling (element) + hot pressing	1.3	348-373 K	Ref. [25]
$Bi_{0.3}Sb_{1.7}Te_3$	Ball milling + SPS + nano-SiC	1.33	373 K	Ref. [8]
$BiSbTe_3$	Hydrothermal + hot pressing	1.47	443 K	Ref. [26]
$Bi_{0.5}Sb_{1.5}Te_3$	High-pressure synthesis (3.8 GPa)	1.3	510 K	Ref. [27]
$Bi_{0.6}Sb_{1.4}Te_3$	Pressure-quenching (HPHT, 4 GPa) + CNTs	1.42	373 K	This work

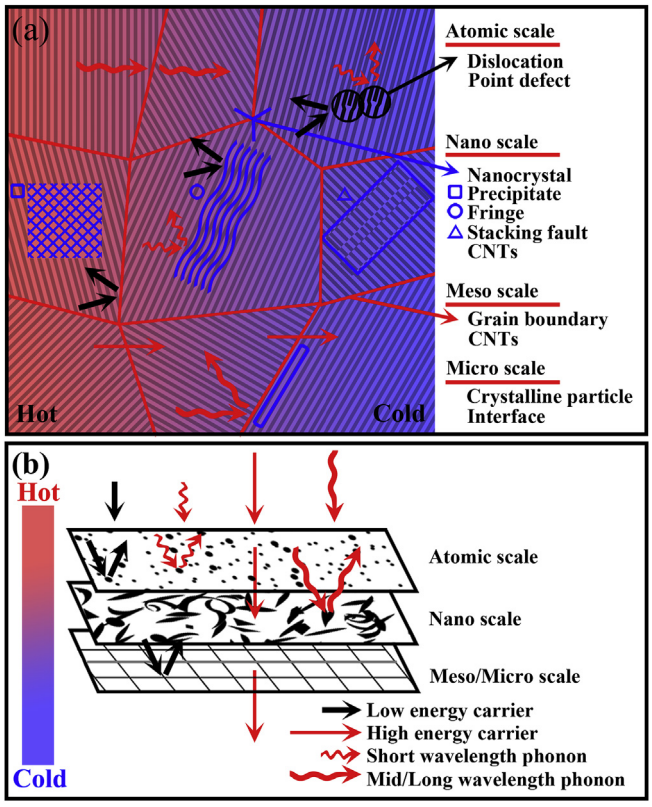

Fig. 8. Schematic of low energy carrier filtering and phonon scattering mechanism from hot to cold junction.

nanoscale originate from rapid crystal growth, inhomogeneity, and lattice distortions; **(3) Meso scale**, including boundaries and interfaces. Grain boundaries and amorphous regions restrain low-frequency/long-wavelength phonons with frequency-dependent relaxation time of $\tau_B^{-1} \sim \omega^0$; and **(4) Micro scale**. The grain particles and interfaces of CNTs can also scatter low-frequency/long-wavelength phonons (ω^0). Besides, typical Umklapp scattering shows the frequency dependence of relaxation time: $\tau_U^{-1} \sim \omega^2$. Therefore, there are many mid-frequency heat-carrying phonons contributing to thermal conductivity. In our work, the extensive meso scale microstructures can exactly target the broad range of mid-frequency/mid-to-long wavelength phonons (from ω^1 to ω^3). Various microstructures can scatter the corresponding phonon modes, resulting in the reduction of relaxation time and mean free path. Also, high-energy carriers are capable to get through the microstructures, which is beneficial to enhance the Seebeck coefficient. Clearly, pressure-quenching method can achieve full-spectrum phonon scattering, which should be responsible for the low thermal conductivity.

4. Conclusion

The HPHT quenching method was applied to fabricate CNTs-composited BiSbTe nanostructured bulk material with the nanocrystals and multiple microstructures. The more interfaces and phase boundaries appeared in the CNTs composite. The multiscale interfaces could distinctly decrease the thermal conductivity by full-spectrum-phonons scattering and enhance the Seebeck coefficient by low energy carrier filtering effect. The maximum ZT value of 1.42 at 373 K was obtained. The improvement of the ZT value was ascribed to the microstructures arising from quenching from a higher synthetic pressure. It could be expected to further improve the ZT value by optimizing the dimension distribution of microstructures corresponding to various phonon modes.

Acknowledgements

This work was financially supported by National Natural Science Foundation of China (No. 51171070 and No. 51071074).

References

[1] Bell LE. Cooling, heating, generating power, and recovering waste heat with thermoelectric systems. Science 2008;321:1457–61.
[2] Lan Y, Minnich AJ, Chen G, Ren Z. Enhancement of thermoelectric figure-of-merit by a bulk nanostructuring approach. Adv Funct Mater 2010;20:357–76.
[3] Pei Y, Wang H, Snyder G. Band engineering of thermoelectric materials. Adv Mater 2012;24:6125–35.
[4] Li JF, Liu WS, Zhao LD, Zhou M. High-performance nanostructured thermoelectric materials. NPG Asia Mater 2010;2:152–8.
[5] Vineis CJ, Shakouri A, Majumdar A, Kanatzidis MG. Nanostructured thermoelectrics: big efficiency gains from small features. Adv Mater 2010;22:3970–80.
[6] Venkatasubramanian R, Siivola E, Colpitts T, O'quinn B. Thin-film thermoelectric devices with high room-temperature figures of merit. Nature 2001;413:597–602.
[7] Harman T, Taylor P, Walsh M, LaForge B. Quantum dot superlattice thermoelectric materials and devices. Science 2002;297:2229–32.
[8] Li J, Tan Q, Li JF, Liu DW, Li F, Li ZY, et al. BiSbTe-based nanocomposites with high ZT: the effect of SiC nanodispersion on thermoelectric properties. Adv Funct Mater 2013;23:4317–23.
[9] Zhao X, Ji X, Zhang Y, Zhu T, Tu J, Zhang X. Bismuth telluride nanotubes and the effects on the thermoelectric properties of nanotube-containing nanocomposites. Appl Phys Lett 2005;86:062111.
[10] Yu HD, Regulacio MD, Ye E, Han MY. Chemical routes to top-down nanofabrication. Chem Soc Rev 2013;42:6006–18.
[11] Zhu T, Xu Z, He J, Shen J, Zhu S, Hu L, et al. Hot deformation induced bulk nanostructuring of unidirectionally grown p-type (Bi, Sb)2Te3 thermoelectric materials. J Mater Chem A 2013;1:11589–94.
[12] Xie W, Tang X, Yan Y, Zhang Q, Tritt TM. Unique nanostructures and enhanced thermoelectric performance of melt-spun BiSbTe alloys. Appl Phys Lett 2009;94:102111.
[13] Yao B, Ding B, Sui G, Wang A, Hu Z. Effect of high pressure on the preparation of Pd–Si–Cu bulk nanocrystalline material. J Mater Res 1996;11:912–6.
[14] Schröder T, Schneider MN, Rosenthal T, Eisele A, Gold C, Scheidt EW, et al. Nanostructures in metastable $GeBi_2Te_4$ obtained by high-pressure synthesis and rapid quenching and their influence on physical properties. Phys Rev B 2011;84:184104.
[15] Kim KT, Choi SY, Shin EH, Moon KS, Koo HY, Lee GG, et al. The influence of CNTs on the thermoelectric properties of a CNT/Bi_2Te_3 composite. Carbon 2013;52:541–9.
[16] Gothard N, Tritt TM, Spowart J. Figure of merit enhancement in bismuth telluride alloys via fullerene-assisted microstructural refinement. J Appl Phys 2011;110:023706.
[17] Zhang Y, Jia X, Deng L, Guo X, Sun H, Sun B, et al. Evolution of thermoelectric properties and anisotropic features of Bi_2Te_3 prepared

by high pressure and high temperature. J Alloys Compd 2015;632:514–9.
[18] Xie W, He J, Zhu S, Holgate T, Wang S, Tang X, et al. Investigation of the sintering pressure and thermal conductivity anisotropy of melt-spun spark-plasma-sintered $(Bi,Sb)_2Te_3$ thermoelectric materials. J Mater Res 2011;26:1791–9.
[19] Snyder GJ, Toberer ES. Complex thermoelectric materials. Nat Mater 2008;7:105–14.
[20] Li D, Wang A, Yao B, Ding B, Hu Z. Synthesis of bulk nanocrystalline Ti–Cu alloy by pressure-quenching method. J Mater Res 1996;11:2685–8.
[21] Liu WS, Zhang BP, Li JF, Zhang HL, Zhao LD. Enhanced thermoelectric properties in $CoSb_{3-x}Te_x$ alloys prepared by mechanical alloying and spark plasma sintering. J Appl Phys 2007;102:103717.
[22] Hu LP, Zhu TJ, Wang YG, Xie HH, Xu ZJ, Zhao XB. Shifting up the optimum figure of merit of p-type bismuth telluride-based thermoelectric materials for power generation by suppressing intrinsic conduction. NPG Asia Mater 2014;6:e88.
[23] Kim SI, Lee KH, Mun HA, Kim HS, Hwang SW, Roh JW, et al. Dense dislocation arrays embedded in grain boundaries for high-performance bulk thermoelectrics. Science 2015;348:109–14.
[24] Poudel B, Hao Q, Ma Y, Lan Y, Minnich A, Yu B, et al. High-thermoelectric performance of nanostructured bismuth antimony telluride bulk alloys. Science 2008;320:634–8.
[25] Ma Y, Hao Q, Poudel B, Lan Y, Yu B, Wang D, et al. Enhanced thermoelectric figure-of-merit in p-type nanostructured bismuth antimony tellurium alloys made from elemental chunks. Nano Lett 2008;8:2580–4.
[26] Cao Y, Zhao X, Zhu T, Zhang X, Tu J. Syntheses and thermoelectric properties of Bi_2Te_3/Sb_2Te_3 bulk nanocomposites with laminated nanostructure. Appl Phys Lett 2008;92:143106.
[27] Guo X, Jia X, Qin J, Sun H, Zhang Y, Sun B, et al. Fast preparation and high thermoelectric performance of the stable $Bi_{0.5}Sb_{1.5}Te_3$ bulk materials for different synthesis pressures. Chem Phys Lett 2014;610:204–8.
[28] Toberer ES, Zevalkink A, Snyder GJ. Phonon engineering through crystal chemistry. J Mater Chem 2011;21:15843–52.
[29] Minnich A, Dresselhaus M, Ren Z, Chen G. Bulk nanostructured thermoelectric materials: current research and future prospects. Energy & Environ Sci 2009;2:466–79.
[30] Saleemi M, Toprak MS, Li S, Johnsson M, Muhammed M. Synthesis, processing, and thermoelectric properties of bulk nanostructured bismuth telluride (Bi_2Te_3). J Mater Chem 2012;22:725–30.

Yuewen Zhang is a graduate student in National Key Lab of Superhard Materials at Jilin University. His researches focus on the synthesis and performance optimization of thermoelectric materials (Bi_2Te_3 and SnSe) by high pressure and high temperature method.